

The role of inner-shell excitations in electron recombination with complex multicharged ions

S. Sahoo and G. F. Gribakin

Department of Applied Mathematics and Theoretical Physics, Queen's University,
Belfast BT7 1NN, UK

Abstract. We performed an overview of the inner shell excitation phenomena in the study of electron recombination with multiply charged complex ions such as Au^{q+} ($q=49-52$) and Pb^{53+} . It is found that the inner shell excitations play a significant role in the low energy electron recombination. Taking into account these inner shell excitations we have calculated the energy averaged capture cross sections. The dielectronic rate coefficients are found to be in good agreement with the experiment. We show that the contribution from the inner-shell enhances the recombination rate by an order of magnitude. We also made an attempt to identify the resonances observed by the experiment in Au^{50+} and Pb^{53+} . A prediction is made for the rate enhancement in Au^{52+} in which we found the configuration mixing between the doubly and the complex multiply excited states. Analyzing the statistics of eigenstate components we estimated the spreading width is about 0.85 a.u. which defines the energy range within which strong mixing takes place.

PACS numbers: PACS: 34.80.Lx, 31.10.+z, 34.10.+x, 32.80.Dz

1. Introduction

The electron recombination process has been the most thoroughly studied problem in the present era due to its practical importance in different areas of modern physics. In particular dielectronic recombination (DR) process is one of the important recombination process in high temperature plasmas. Accurate DR rate coefficients are needed for successful modeling of astrophysical and laboratory plasmas. The current interest in study of the DR is the rate enhancement in the recombination of low energy electron with multiply charged complex ions. This enhancement phenomena was first observed by Muller et al. [1] in U^{28+} ion. The interest in the rate enhancement is largely due to the importance of understanding the mechanism of recombination in particular those involving multiply charged complex ions. Apart from this the potential application in the production of antihydrogen by recombination of an antiproton with positrons has provided a great deal of stimulus to study the detailed mechanism of the DR process [2]. The main feature in the rate enhancement is that at low energy, the

measured recombination rate coefficients significantly exceed the theoretical predictions for radiative recombination (RR). In the higher energies, measured rates are well explained by RR theory together with contribution of DR.

The complex ions such as Au^{25+} [3], Au^{50+} [4] and Pb^{53+} [5, 6] show a strongly enhanced recombination rate. In Au^{25+} ion the rate enhancement has been justified by Gribakin et. al.[7] and Flambaum et. al.[8] using a statistical approach. They showed that the electron capture is mediated by complex multiply excited states rather than simple dielectronic resonances in this system. In a recent study Gribakin et. al. [9] have explained the detailed mechanism responsible for low energy rate enhancement in U^{28+} . In this system these authors reported that the mechanism lies behind the fact that doubly excited configurations mix with each other weakly and they do mix with the complex multiply excited states quite comfortably. Most importantly the excitations from inner shell hole plays a major role in the low electron energies which was absent in the calculation of Mitnik et al [10] and is unable to produce the results in agreement with the experiment in the low electron energies. For Pb^{53+} ion, Lindorth et al [6] performed a comprehensive study to calculate the resonances using relativistic perturbation theory. They found on comparison with the experiment, the energy splitting in $\text{Pb}^{53+}(4p_{1/2}-4s_{1/2})$ with an accuracy comparable to the position of first few resonances and concluded that such an accuracy provides a test of QED in many body systems. Although these authors are able to identify the resonances with a very good precision, their theoretical values for recombination rate still need an improvement in order to be in good agreement with the measured data. This system is of the current interest in the present study along with another similar system i.e., Au^{50+} since there is no theory for this particular system. In order to achieve a clearer understanding we have also investigated the nearest neighbouring ions such as $\text{Au}^{49+,51+,52+}$. In the present calculation we have included the excitations from the inner shells and found that the results are significantly improved with this inclusion. The importance of the inner shell excitation in the low energy electron recombination in U^{28+} has already been established [9]. Moreover, a recent study on bound doubly excited states formation when slow highly charged ions ($\text{Ta}^q, q = 39-48$) capture a single electron in collision with He by Schuch et. al.[11] reports that they observed a strong characteristic M x-Ray emission without an M shell vacancy initially present. In the present article we present the results of recombination rates for the above mentioned ions taking into account the inner shell vacancy. We compare these results with the available calculations that do not take into account the inner shell excitations. A good agreement has been achieved in comparison with the available experimental data as well.

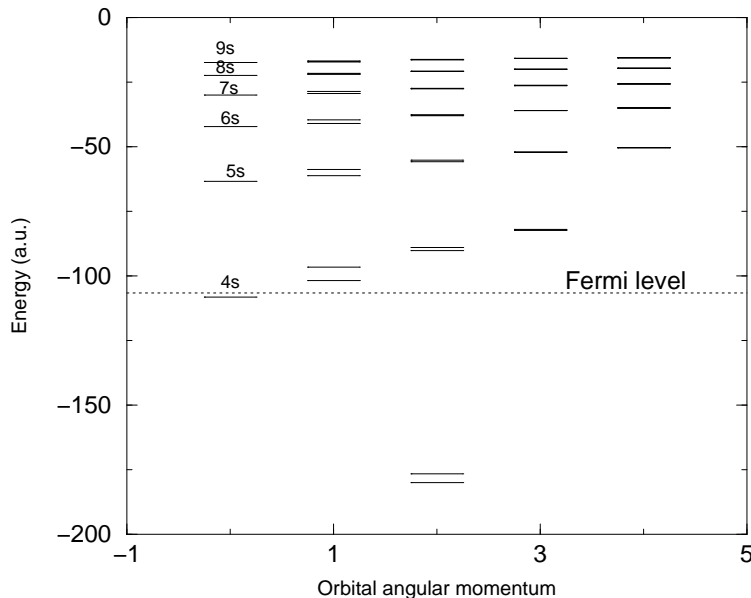
2. Many-electron excitations

Ref. [7, 8] suggest that electron recombination with complex multiply charged ions is mediated by complex *multiply-excited* states of the compound ions (target+e) rather than “simple” dielectronic resonances. Electrons could be captured in these states due

Table 1. Ground state energy and Ionization threshold (I) of different ions.

Ground state Energy (a.u.)			
q	Au^{q+}	$\text{Au}^{(q-1)+}$	I(a.u.)
49	17287.64	17387.22	99.58
50	17181.91	17287.56	105.65
51	17073.75	17181.90	108.15
52	16894.25	17073.60	179.35
	Pb^{q+}	$\text{Pb}^{(q-1)+}$	I(a.u.)
53	18742.07	18860.26	118.19

to a strong configuration interaction. The ground state of Au^{q+} for $(q = 49 - 51)$ is described by the $1s^2 \dots 3d^{10}4s^k (k = 0, 1, 2)$ configuration and for $\text{Au}^{q+} (q = 52)$, it is described by $1s^2 \dots 3d^k (k = 9)$ configuration. Similarly for $\text{Pb}^{q'} (q' = 53)$, the ground state configuration is $1s^2 \dots 3d^{10}4s^k (k = 1)$. Figure 1 shows the spectrum of relativistic single-particle orbitals of $\text{Au}^{q+} (q = 50)$. The occupied orbitals (below the Fermi level) are obtained in a relativistic Dirac-Fock calculation of the Au^{q+} ground state, and the excited state orbitals (above the Fermi level) are obtained by solving the Dirac-Fock equation for an electron in the potential of $\text{Au}^{25+} 1s^2 \dots 4s^1$ core. Table 1 shows the ground state energy obtained from configuration interaction (CI) calculation for different targets and the compound ions. The difference between the total energies


Figure 1. Energies of occupied and vacant single-particle orbitals of Au^{50+} obtained in a Dirac-Fock calculation.

of the target ions and their respective compound ions gives us the ionization threshold which is shown in table I. Since we are interested near the ionization threshold, we

consider 3p orbitals are inactive and allowed the orbitals from 3d onwards to take active part in the process. We distributed these active electron among 61 relativistic orbitals from $3d_{3/2}$ to $9g_{7/2}$. We construct the excitation spectrum of $\text{Au}^{(q-1)+}$ and $\text{Pb}^{(q'-1)+}$ by calculating the mean energies E_i , and number of many electron states N_i :

$$E_i = E_{core} + \sum_a \epsilon_a n_a + \sum_{a < b} \frac{n_a (N_b - \delta_{ab})}{1 + \delta_{ab}} U_{ab}, \quad (1)$$

$$N_i = \prod_a \frac{g_a!}{n_a! (g_a - n_a)!}, \quad (2)$$

where n_a are the orbital occupation numbers of the relativistic orbitals in a given configuration and $\sum_a n_a = n$. $\epsilon_a = \langle a | H_{core} | a \rangle$ is the single-particle energy of the orbital a in the field of the core, $g_a = 2j_a + 1$, and U_{ab} are the average Coulomb matrix elements for the electrons in orbitals a and b (direct minus exchange):

$$U_{ab} = \frac{g_a}{g_a - \delta_{ab}} \left[R_{abab}^{(0)} - \sum_{\lambda} \delta_p R_{abba}^{(\lambda)} \left\{ \begin{matrix} j_a & j_b & \lambda \\ \frac{1}{2} & -\frac{1}{2} & 0 \end{matrix} \right\}^2 \right] \quad (3)$$

$R_{abba}^{(\lambda)}$ is the two-body radial Coulomb integral of λ multipole, and $\delta_p = 1$ when $l_a + l_b + \lambda$ is even and 0 otherwise. Using the single-particle orbitals we have generated many-electron configurations, evaluated their energies and estimated the energy density of multiply-excited states [7].

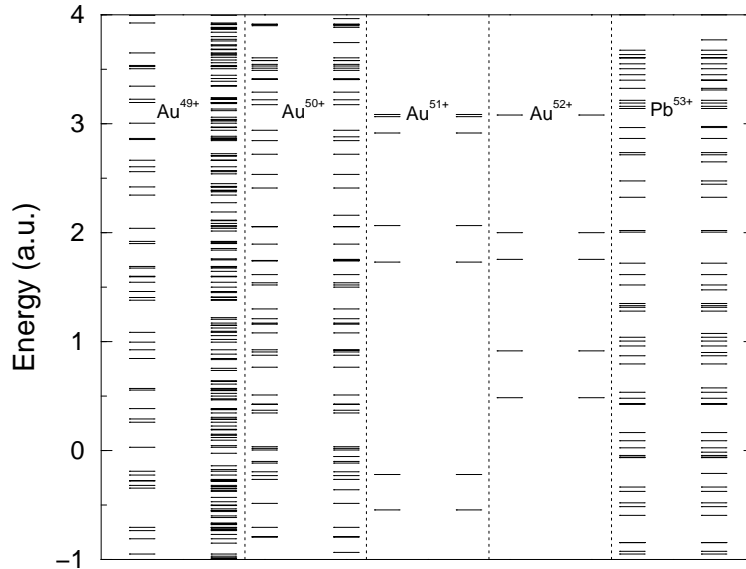


Figure 2. Position of the dielectronic and multiply excited states of ions with respect to their ionization threshold (see table I).

Figure 2 shows the doubly excited states as well as multiply excited states near the ionization threshold of the ions. We plotted all the configurations having energies between -1 and 4 a.u.. In Au^{49+} , there is only one doubly excited state near the ionization

threshold although a significant number of multiply excited states are found nearby this particular dielectronic state. It is also found that the multiply excited states are not populated through this state and hence rate enhancement is not expected, which has been explained by the experiment[4]. In case of Au^{51+} , we did not find any dielectronic states near its ionization threshold. However, Au^{50+} and Pb^{53+} , shows a number of dielectronic states near its ionization threshold and these contribute largely to the rate enhancement. Au^{52+} shows there are a few dielectronic states above the ionization threshold. It may be mentioned that one may expect rate enhancement in this ion because these dielectronic states shows a substantial mixing with each other. The detailed study of the nature dielectronic states near the ionization threshold of all the ions is discussed later.

3. Recombination

3.1. Theory

For low-energy electrons the contribution of the autoionising states (resonances) to the recombination cross section is given by (see, e.g., Ref. [12])

$$\sigma_r = \frac{\pi}{k^2} \sum_{\nu} \frac{2J+1}{2(2J_i+1)} \frac{\Gamma_{\nu}^{(r)} \Gamma_{\nu}^{(a)}}{(\varepsilon - \varepsilon_{\nu})^2 + \Gamma_{\nu}^2/4}, \quad (4)$$

where $\varepsilon = k^2/2$ is the electron energy, J_i is the angular momentum of the initial (ground) target state, J are the angular momenta of the resonances, $\varepsilon_{\nu} = E_{\nu} - I$ is the position of the ν th resonance relative to the ionization threshold of the compound (final-state) ion, and $\Gamma_{\nu}^{(a)}$, $\Gamma_{\nu}^{(r)}$, and $\Gamma_{\nu} = \Gamma_{\nu}^{(r)} + \Gamma_{\nu}^{(a)}$ are its autoionisation, radiative, and total widths, respectively [13]. When the resonance spectrum is dense, σ_r can be averaged over an energy interval $\Delta\varepsilon$ which contains many resonances, $D \ll \Delta\varepsilon \ll \varepsilon$, yielding

$$\bar{\sigma}_r = \frac{2\pi^2}{k^2} \sum_{J\pi} \frac{2J+1}{2(2J_i+1)D} \left\langle \frac{\Gamma_{\nu}^{(r)} \Gamma_{\nu}^{(a)}}{\Gamma_{\nu}^{(r)} + \Gamma_{\nu}^{(a)}} \right\rangle, \quad (5)$$

where $\langle \dots \rangle$ means averaging. If the fluorescence yield, $\omega_f \equiv \Gamma_{\nu}^{(r)} / (\Gamma_{\nu}^{(r)} + \Gamma_{\nu}^{(a)})$, fluctuates weakly from resonance to resonance (see below), one can write $\bar{\sigma}_r = \bar{\sigma}_c \omega_f$, where

$$\bar{\sigma}_c = \frac{\pi^2}{k^2} \sum_{J\pi} \frac{(2J+1)\Gamma^{(a)}}{(2J_i+1)D} \quad (6)$$

is the energy-averaged capture cross section, and $\Gamma^{(a)}$ is the average autoionisation width.

In a situation when there is a strong configuration mixing between the dielectronic doorway states and multiply excited states, the capture cross sections can be obtained as a sum over the single-electron excited states α , β and hole states γ , as well as the partial waves lj of the continuous-spectrum electron ε . As a result, we have

$$\bar{\sigma}_c = \frac{\pi^2}{k^2} \sum_{\alpha\beta\gamma,lj} \frac{\Gamma_{\text{spr}}}{(\varepsilon - \varepsilon_{\alpha} - \varepsilon_{\beta} + \varepsilon_{\gamma})^2 + \Gamma_{\text{spr}}^2/4} \sum_{\lambda} \frac{\langle \alpha, \beta || V_{\lambda} || \gamma, \varepsilon lj \rangle}{2\lambda + 1}$$

$$\times \left[\langle \alpha, \beta \| V_\lambda \| \gamma, \varepsilon l j \rangle - (2\lambda + 1) \sum_{\lambda'} (-1)^{\lambda+\lambda'+1} \left\{ \begin{matrix} \lambda & j_\alpha & j \\ \lambda' & j_\beta & j_\gamma \end{matrix} \right\} \langle \alpha, \beta \| V_{\lambda'} \| \varepsilon l j, \gamma \rangle \right]$$

where ε_α , ε_β and ε_γ are the orbital energies, the two terms in square brackets represent the direct and exchange contributions, and $\langle \alpha, \beta \| V_\lambda \| \gamma, \varepsilon l j \rangle$ is the reduced Coulomb matrix element.

It is assumed that the energies of dielectronic doorway states relative to the threshold is given by $\varepsilon_\alpha + \varepsilon_\beta - \varepsilon_\gamma$. A more accurate value can be obtained by using mean field energies (configuration energies) of doorway configurations in Eq.(10). Therefore we used the configuration energy in the calculation of capture cross sections.

Equation (7) is directly applicable to targets with closed-shell ground states. If the target ground state contains partially occupied orbitals, a factor

$$\frac{n_\gamma}{2j_\gamma + 1} \left(1 - \frac{n_\alpha}{2j_\alpha + 1} \right) \left(1 - \frac{n_\beta}{2j_\beta + 1} \right), \quad (8)$$

where n_α , n_β , and n_γ are the orbital occupation numbers in the ground state Φ_i , must be introduced on the right-hand side of Eq. (7). Steps similar to those that lead to Eq. (7) were used to obtain mean-squared matrix elements of operators between chaotic many-body states [14, 15].

The chaotic nature of the multiply-excited states Ψ_ν can also be employed to estimate their radiative widths $\Gamma_\nu^{(r)}$. Electron-photon interaction is described by a single-particle dipole operator \hat{d} . Any excited electron in Ψ_ν may emit a photon, thus leading to radiative stabilization of this state. The total photo-emission rate $\Gamma_\nu^{(r)}$ can be estimated as a weighted sum of the single-particle rates,

$$\Gamma_\nu^{(r)} \simeq \sum_{\alpha, \beta} \frac{4\omega_{\beta\alpha}^3}{3c^3} |\langle \alpha \| \hat{d} \| \beta \rangle|^2 \left\langle \frac{n_\beta}{2j_\beta + 1} \left(1 - \frac{n_\alpha}{2j_\alpha + 1} \right) \right\rangle_\nu, \quad (9)$$

where $\omega_{\beta\alpha} = \varepsilon_\beta - \varepsilon_\alpha > 0$, $\langle \alpha \| \hat{d} \| \beta \rangle$ is the reduced dipole operator between the orbitals α and β , and $\langle \dots \rangle_\nu$ is the mean occupation number factor. Since Ψ_ν have large numbers of principal components N , their radiative widths display small $1/\sqrt{N}$ fluctuations. This can also be seen if one recalls that a chaotic multiply-excited state is coupled by photo-emission to many lower-lying states, and the total radiative width is the sum of a large number of (strongly fluctuating) partial widths. A similar effect is known in compound nucleus resonances in low-energy neutron scattering [16].

There is a certain similarity between Eqs. (7) and (9) and those for autoionisation and radiative rates obtained in a so-called configuration-average approximation [17]. In both cases the answers involve squares or products of two-body Coulomb matrix elements [see the direct and exchange terms in Eq. (7)], or single-particle dipole amplitudes [Eq. (9)]. However, there are a number of important differences between the present results and the configuration-average approximation. The latter considers dielectronic recombination and introduces averaging over configurations as a means of simplifying the calculation. The DR cross section is averaged over an arbitrary energy interval $\Delta\varepsilon$, and only the configurations within this energy range contribute to the

average. Effects of configuration mixing as well as level mixing within a configuration are neglected.

It is important to compare the radiative and autoionisation widths of chaotic multiply-excited states. Equation (9) shows that $\Gamma^{(r)}$ is comparable to the single-particle radiative widths. On the other hand, the autoionisation width $\Gamma^{(a)}$, is suppressed by a factor $\left|C_k^{(\nu)}\right|^2 \sim N^{-1}$ relative to that of a typical dielectronic resonance. Therefore, in systems with dense spectra of chaotic multiply-excited states the autoionisation widths are small. Physically this happens because the coupling strength of a two-electron doorway state to the continuum is shared between many complicated multiply-excited eigenstates. As a result, the radiative width may dominate the total width of the resonances, $\Gamma^{(r)} \gg \Gamma^{(a)}$, making their fluorescence yield close to unity.

The resonance recombination cross section should be compared with the direct radiative recombination cross section

$$\sigma_d = \frac{32\pi}{3\sqrt{3}c^3} \frac{Z_i^2}{k^2} \ln \left(\frac{Z_i}{n_0 k} \right), \quad (10)$$

obtained from the Kramers formula by summing over the principal quantum number of the final state [7]. Note that the direct and energy-averaged resonance recombination cross sections of Eqs. (10) and (5) have similar energy dependences.

3.2. Numerical results

Au⁴⁹⁺

We present the RR and DR rate coefficients for Au⁴⁹⁺ in figure 3 in the energy range between 0 to 100 eV. We also included in the same figure the dielectronic configurations producing the resonances and are by solid vertical lines. The position of peaks in the DR rate corresponds to each of the doubly excited states. It is evident from the figure that there is no strong dielectronic configurations near

the ionization threshold and hence the experiment does not show an enhancement in the rate coefficients as well as resonance structure in the low energies. We found the only isolated doubly excited state near the threshold involves 4s excitation is not particularly strong. However, at higher electron energies, quite a number of resonances are observed. Of particular importance are the dielectronic states those produce larger peaks. We identified them as the states which involve the inner shell hole. These states are indicated with the numbers (1,2,3 etc) in the figure. One of such states found to appear around 40 eV is $3d_{3/2}^4 3d_{5/2}^5 4s_{1/2}^2 4d_{3/2}^1 4f_{5/2}^1$ due to which a large peak is observed. We found in the present ion, these type of configurations give most contribution to the recombination rate. Identifying these type of configuration we plotted them with respect to the ionization threshold in Fig.8. It appears that configurations are far above the ionization threshold i.e above 40 eV. To get more evidence if they produce any low energy resonance we performed a configuration calculation taking only these type of configurations into account. We obtained the excited spectrum for all total angular

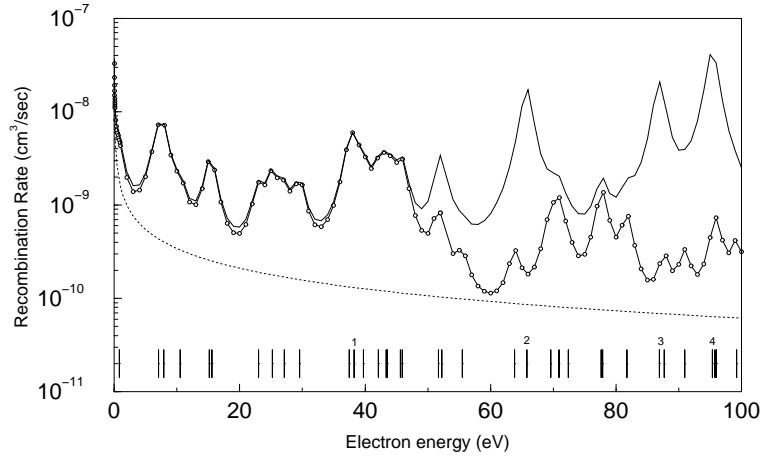


Figure 3. Recombination rate in Au^{49+} . dotted line: RR rate, solid line: DR rate with a hole in inner shell (3d), open circles connected by solid line: DR rate without inner shell excitation and solid vertical lines numbered 1-4: position of dielectronic states involving inner shell hole. 1: $3d_{3/2}^4 3d_{5/2}^5 4s_{1/2}^2 4d_{3/2}^1 4f_{5/2}^1$, 2: $3d_{3/2}^4 3d_{5/2}^5 4s_{1/2}^2 4d_{3/2}^1 4f_{7/2}^1$, 3: $3d_{3/2}^4 3d_{5/2}^5 4s_{1/2}^2 4d_{5/2}^1 4f_{5/2}^1$, 4: $3d_{3/2}^4 3d_{5/2}^5 4s_{1/2}^2 4d_{3/2}^1 4f_{7/2}^1$.

momentum J resulted from diagonalization of configuration Hamiltonian. These are plotted as a function of eigen energies ranging from -4 to 4 a.u. in Fig.9 and -2 to 2 eV in Fig.10. We found some resonances but they are not particularly strong in nature. It is also interesting to note that we performed a calculation without including the inner shell excitations. The results of rate coefficients are shown by circles connected by solid lines. This shows that the inner shell excitations in this ion plays a crucial role in the high electron energies and at low electron energies a negligible effect is found. This because the configurations are positioned in the higher electron energies (fig. 8).

Au^{51+}

For the case of Au^{51+} we found practically no dielectronic states near its ionization threshold. As mentioned earlier large contributions to the capture cross sections comes from the dielectronic states involving the inner shell hole (3d) and 4d and 4f excited orbitals, these are found to be in either side of the ionization threshold. This may be seen in Fig.4 where we have shown the recombination rate (fig. 8). Figure 9 and figure 10 also indicate that there is not even a single resonance around the threshold. At low energies the DR and RR rates are nearly equal. At higher energies the enhancement in DR rate is found due to the presence of configurations involving the inner shell hole. The position of each peaks in the DR rate coefficients corresponds to the position of dielectronic configurations and are indicated by vertical solid lines.

Au^{50+}

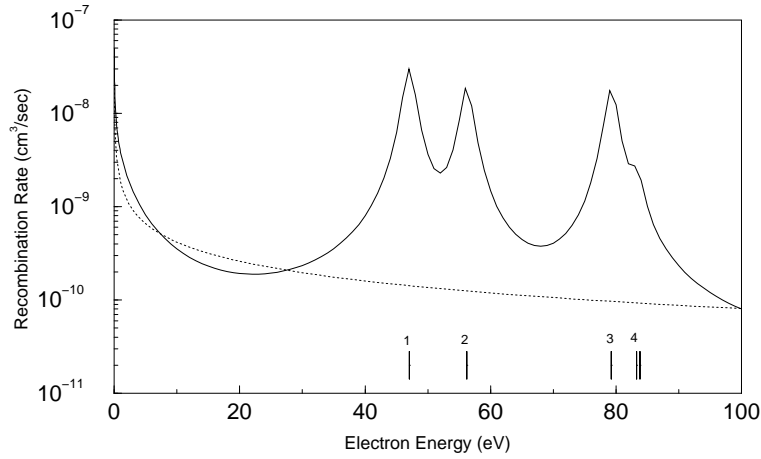


Figure 4. Recombination rate in Au^{51+} . dotted line: RR rate, solid line: DR rate. Vertical lines with numbers 1-4 indicate the position of configurations involving inner shell hole. 1: $3d_{3/2}^3 3d_{5/2}^6 4d_{3/2}^1 4f_{5/2}^1$, 2: $3d_{3/2}^3 3d_{5/2}^6 4d_{3/2}^1 4f_{7/2}^1$, 3: $3d_{3/2}^3 3d_{5/2}^6 4d_{5/2}^1 4f_{5/2}^1$, 4: $3d_{3/2}^3 3d_{5/2}^6 4d_{5/2}^1 4f_{7/2}^1$.

Now we present the interesting results for Au^{50+} in figure 5. We found there is a low energy DR rate enhancement which is in agreement with experiment.

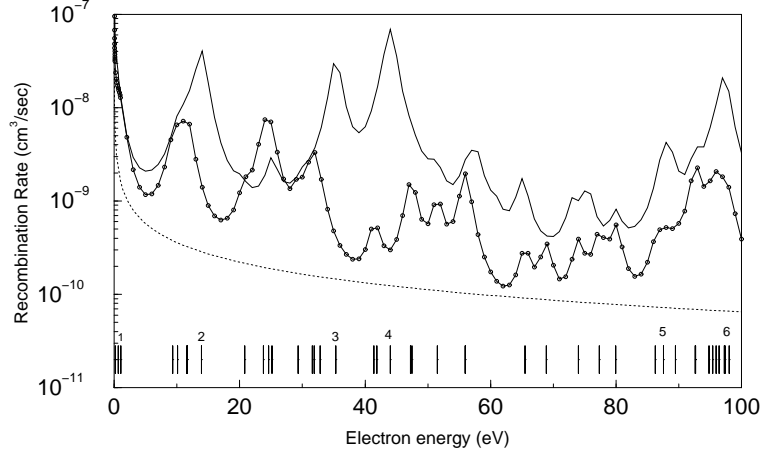


Figure 5. Recombination rate in Au^{50+} . dotted line: RR rate, solid line: DR rate with a hole in inner shell (3d), open circles connected by solid line: DR rate without inner shell excitation and solid vertical lines numbered 1-6 : position of dielectronic states involving the inner shell hole. 1: $3d_{3/2}^4 3d_{5/2}^5 4s_{1/2}^1 4d_{3/2}^1 4f_{5/2}^1$, 2: $3d_{3/2}^4 3d_{5/2}^5 4s_{1/2}^1 4d_{3/2}^1 4f_{7/2}^1$, 3: $3d_{3/2}^4 3d_{5/2}^5 4s_{1/2}^1 4d_{5/2}^1 4f_{5/2}^1$, 4: $3d_{3/2}^4 3d_{5/2}^5 4s_{1/2}^1 4d_{3/2}^1 4f_{7/2}^1$, 5: $3d_{3/2}^3 3d_{5/2}^6 4s_{1/2}^1 4d_{3/2}^1 4f_{5/2}^1$, 6: $3d_{3/2}^3 3d_{5/2}^6 4s_{1/2}^1 4d_{3/2}^1 4f_{7/2}^1$.

Also we show a lots of structures and huge peaks in higher electron energies. We identified these peaks and found they correspond to the doubly excited states involving inner shell excitation. The huge enhancement is found around the positions of configuration of type 3d4d4f. It will be interesting to look the Fig. 8 where one can see that the configurations of above nature are close to the ionization

threshold and one of such state i.e., $3d_{3/2}^4 3d_{5/2}^5 4s_{1/2}^1 4d_{3/2}^1 4f_{5/2}^1$ is right at 0.01 a.u. above threshold. Due to its presence it is expected that one will obtain higher recombination rate which we justified here. The experiment in the low energy found huge enhancement and around 10 isolated resonances of which 3 resonances are strong. Our configuration interaction calculation shows that these states produce three resonances as shown in Fig. 10 between 0 and 1 eV of electron energy. The hole spectrum is shown in Fig 9. It is also interesting that when we switched off the inner shell excitation in our calculation there is significant change in the magnitude of DR rates throughout the energy range considered. This confirms the importance of inner shell excitations in electron recombination with complex multiply excited states.

Pb⁵³⁺

The schenerio discussed for Au⁵⁰⁺ is even more interesting in the case of Pb⁵³⁺. The recombination rate for this ion is presented in the figure 6. We found that there is huge DR rate enhancement over RR background particularly in the low energy region. The huge peaks in the recombination rate are found to be due to the doubly excited states involving innershell (3d) excitations as indicated earlier. If one looks at the figure 8, one can see that just like Au⁵⁰⁺, in this system one such state ($3d_{3/2}^4 3d_{5/2}^5 4s_{1/2}^1 4d_{5/2}^1 4f_{5/2}^1$) is positioned at 0.03 a.u. above ionization threshold and the rest configuration of this kind are above and below the ionization threshold.

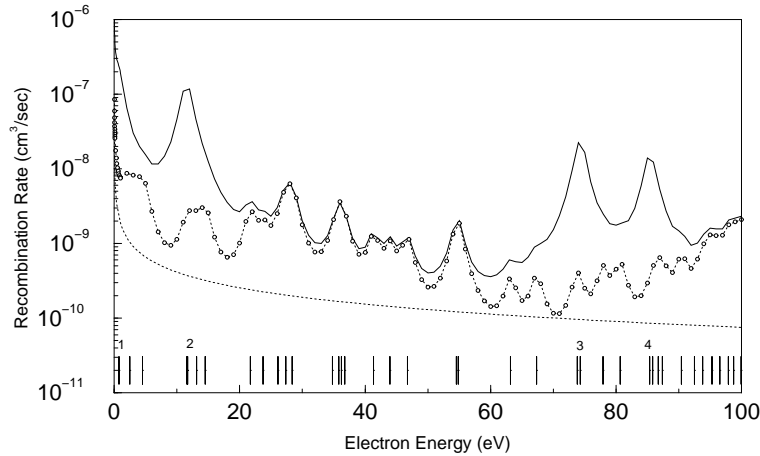


Figure 6. Recombination rate in Pb⁵³⁺. dotted line: RR rate, solid line: DR rate with a hole in inner shell (3d), open circles connected by dotted line: DR rate without inner shell excitation and solid vertical lines numberd 1-4: position of dielectronic states involving innser shell hole.1: $3d_{3/2}^4 3d_{5/2}^5 4d_{5/2}^1 4f_{5/2}^1$, 2: $3d_{3/2}^4 3d_{5/2}^5 4d_{5/2}^1 4f_{7/2}^1$, 3: $3d_{3/2}^3 3d_{5/2}^6 4d_{3/2}^1 4f_{5/2}^1$, 4: $3d_{3/2}^3 3d_{5/2}^6 4d_{3/2}^1 4f_{7/2}^1$.

This configuration at threshold produces huge contributions to the recombination rate in the low energy and hence the enhanced rate as found in the experiment. Another interesting phenomena is that like Au^{Au50}, we also ignore the excitations in

our calculation and the results of which is indicated by small circles connected by solid line. This line lies atleast factor of 10 below the results that includes the inner shell hole especially in the low energy region. It clearly signifies that one can not ignore the inner shell excitations in electron recombination with multiply charged ions. It may be mentioned that the elaborate calculation [6] finds the resonance peaks with a greater accuracy. However, there is still a discrepency in magnitude in comparison to the experimental data. They have taken all the rydberg series into account and their ground state configuration does not include any inner shell hole. To have close look at their results we compared the present results in the low energy region between 0 to 0.1 eV electron energy with the experimeental data [6] as shown in figure 7.

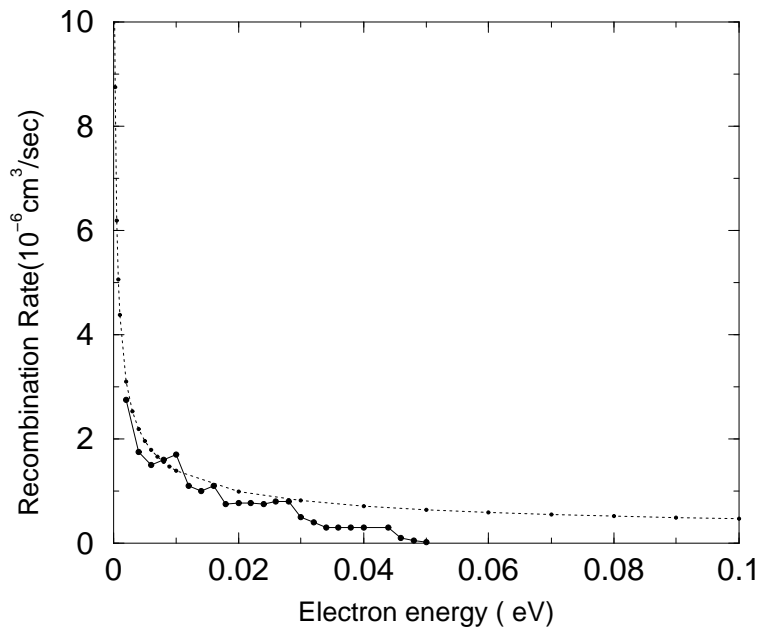


Figure 7. DR rate of Pb^{53+} . Squares connexted by dotted line: Experimenatl data [6], circles connected by solid line : Present calculation.

It may be seen that the presnt results are found to be in resonably good agreement with the experiment.

Au^{52+}

We present the new results for recombination rate of Au^{52+} . Figure 11 shows the recombination rates as a function of electron energy. We also display the position of the dielectronic states by vertical lines those corresponds to each of peaks. In figure 2 we plot the dielectronic as well as multiply excited states in the energy range of -1 to 4 a.u. with respect to the ionization threshold (table 1) of this ion. It may be seen that there are not many doubly excite states so as multiply excited states near the ionization threshold. However, similar to the other ions discussed above we found the dielectronic configutrations involving an inner shell excitations of type

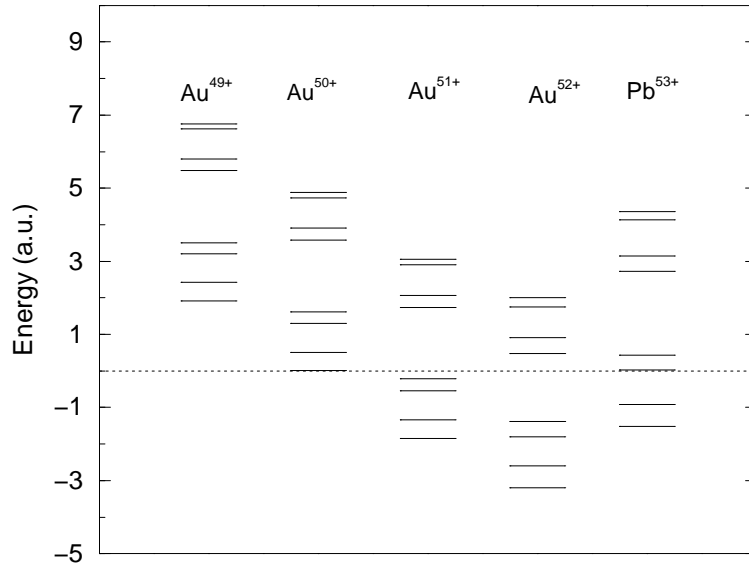


Figure 8. Configurations near the ionization threshold ions involving only 3d holes. In each of the cases top four horizontal lines indicate $3d_{3/2}^3$ excitations with $4d44$ and the bottom four lines represent the position of the configurations involving $3d_{5/2}^5$ excitations with $4d4f$.

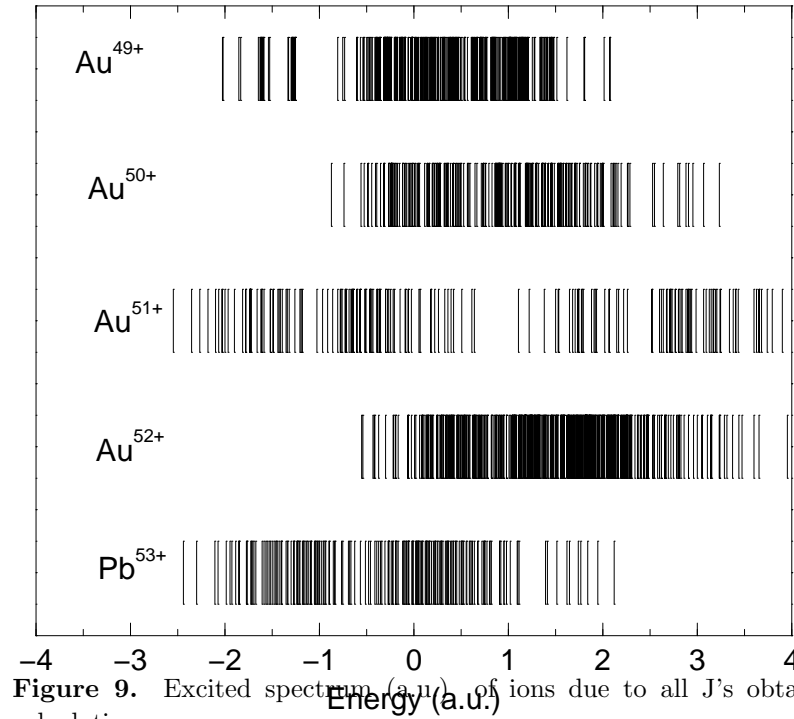


Figure 9. Excited spectrum (a.u.) of ions due to all J's obtained from the CI calculation.

$3d_{3/2}^3 3d_{5/2}^5 4d_{3/2}^1 4f_{5/2}^1$ or $3d_{3/2}^4 3d_{5/2}^4 4d_{3/2}^1 4f_{5/2}^1$ contributes most to the recombination rates. Their positions are far above and below the ionization threshold (Fig.8) and the closest being around 0.5 a.u. (~ 13.6 eV) above the ionization threshold. Their contribution can be seen in the recombination rate indicated by dashed lines connected by open circles. Please note that this calculation uses an arbitrary spreading width ~ 0.75

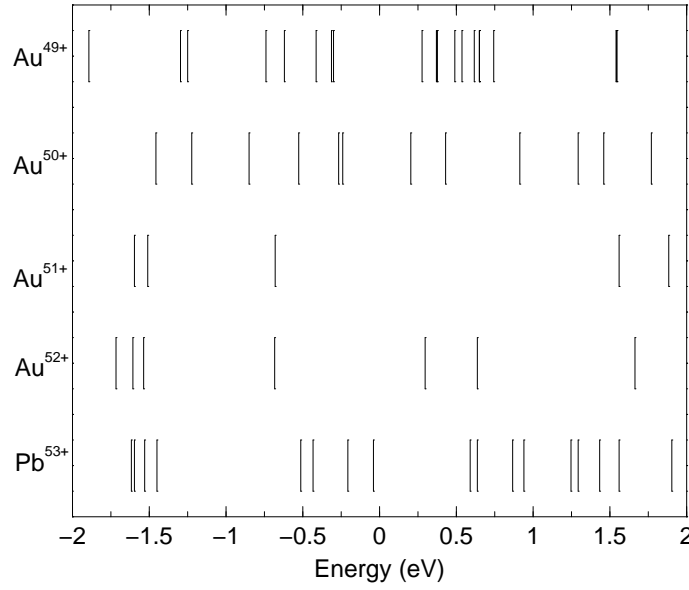


Figure 10. Same as Figure 9 but in eV.

a.u.. Taking these configurations involving inner shell hole we performed a configuration calculation. Our calculation shows that these dielectronic states mix with each other quite comfortably. To study the mixing we plotted the weights of these dielectronic states in Fig. 12. This figure indicates that there is a regular mixing between these states since the weights has gone down significantly from 1. This figure also indicates that these states spread largely on the energy scale. To estimate the spreading width we calculated the mean-squared components and plotted them as a function of basis state energy. The statistics of the meansquared components is well approximated by Breit-Wigner (B-W) formula (Fig. 13). From the BW fitting we estimated the spreading width is 0.85 a.u. which defines the energy range within which strong mixing takes place. In the case of Au^{25+} , it was about 0.5 a.u. [7, 18]. Using this value of the spreading width

we performed another calculation since we believe that this value gives an estimate of the real spreading of the doubly excited states. The results are shown as solid lines in the calculation. The most striking feature in this curve is that there is an enhancement of the DR rate over RR (dotted line). Although the dielectronic states are positioned far from the ionization threshold, but they show a substantial mixing with each other. We believe this mixing leads to an enhancement of DR rate over RR in this ion. It will be more interesting if more theoretical calculations as well as experimental measurements are performed for a complete understanding of this system.

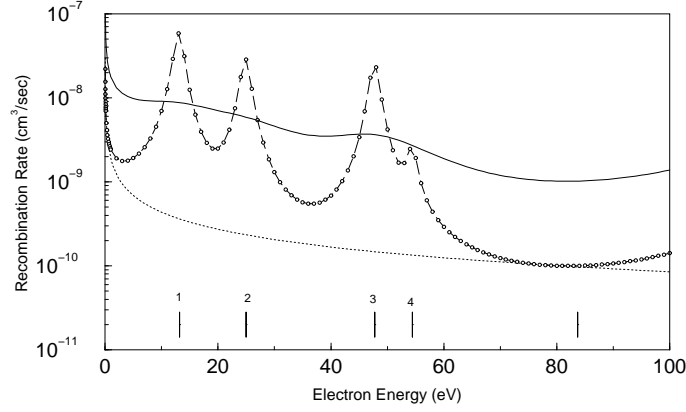


Figure 11. Recombination rate in Au^{52+} . Dotted line: RR rate, solid line DR rate using spreading width 0.85 a.u. and open circles connected by dashed line: DR rate with spreading width 0.75 a.u.. The vertical lines numbered 1 - 4 indicate the position of the doubly excited states involving inner shell hole. 1: $3d_{3/2}^3 3d_{5/2}^5 4d_{3/2}^1 4f_{5/2}^1$, 2: $3d_{3/2}^3 3d_{5/2}^5 4d_{3/2}^1 4f_{7/2}^1$, 3: $3d_{3/2}^3 3d_{5/2}^5 4d_{5/2}^1 4f_{5/2}^1$ and 4: $3d_{3/2}^3 3d_{5/2}^5 4d_{5/2}^1 4f_{7/2}^1$.

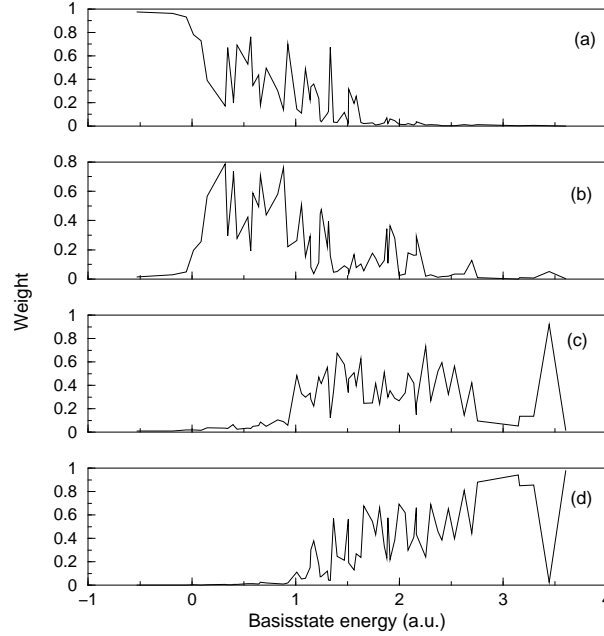


Figure 12. Weights of dielectronic states. (a): $3d_{3/2}^3 3d_{5/2}^5 4d_{3/2}^1 4f_{5/2}^1$, (b): $3d_{3/2}^3 3d_{5/2}^5 4d_{3/2}^1 4f_{7/2}^1$, (c): $3d_{3/2}^3 3d_{5/2}^5 4d_{5/2}^1 4f_{5/2}^1$ and (d): $3d_{3/2}^3 3d_{5/2}^5 4d_{5/2}^1 4f_{7/2}^1$.

4. Summary and outlook

In summary, we find the inner shell excitations play a major role in electron recombination with multiply charged complex ions. The inclusion of the inner shell hole significantly changes the magnitude of DR rates throughout the energy range considered. In U^{28+} , a similar observation has been reported by us [9]. However, we found in Au^{50+} and Pb^{53+} the dielectronic configurations involving an inner shell hole

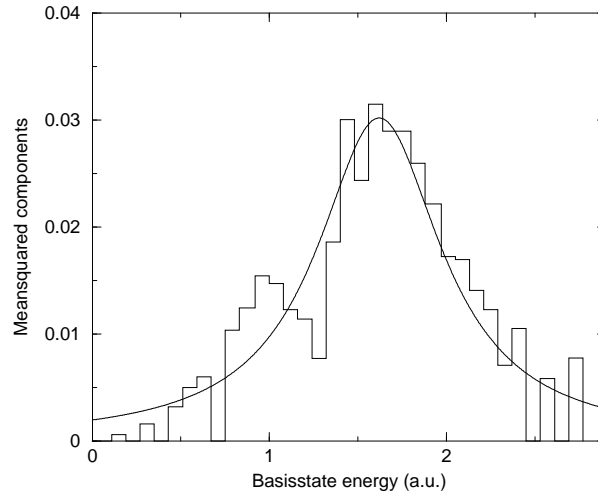


Figure 13. Meansquared components avaraged over 11 neighbouring eigen state components taken from the middle of 69 state CI calculation. The solid line is the BW fit whic estimates the spreading width is 0.85 a.u..

(either $3d^{3/3}$ or $3d^{5/2}$) are positioned very close to the ionization threshold and are responsible for producing higher DR rate over RR in the low electron energies. Also at higher energies due to the presence of these type of configuration an enhancement of DR rate is observed. In Au^{52+} , we made a prediction for the rate enhancement since the dielectronic states show a substantial mixing with each other and associated with a large spreading width ~ 0.85 a.u.. Certainly we invite other theoretical and experimental investigations in order to get a clear understanding of DR process for this system.

5. acknowledgements

We thank Prof. A. Müller for providing experimental data in numerical form.

6. References

- [1] A. Muller *et al.*, Phys. Scr. **T 37**, 62 (1991).
- [2] M. H. Holzschneider and M. Charlton, Rep. Prog. Phys., **61**, 1 (1999).
- [3] A. Hoffknecht *et al.*, J. Phys. B **31**, 2415 (1998) 62 (1991).
- [4] O. Uwira *et al.*, Hyperfine Interact. **108**, 149 (1997).
- [5] S. Biard *et al.*, Phys. Lett. B **361**, 184 (1995).
- [6] E. Lindroth *et al.*, Phys. Rev. Lett. **86**, 5027 (2001).
- [7] G. F. Gribakin, A. A. Gribakina, and V. V. Flambaum, Aust. J. Phys. **52**, 443 (1999); see also physics/9811010.
- [8] V. V. Flambaum *et al.*, Phys. Rev. A **66**, 012713 (2002)
- [9] G. F. Gribakin, S. Sahoo and V. Dzuba, Phys. Rev. A (to be published)
- [10] D. M. Mitnik *et al.*, Phys. Rev. A **57**, 4365 (1998).
- [11] E. Schuch *et al.*, Phys. Rev. Lett. **85**, 5559 (2000)
- [12] L. D. Landau and E. M. Lifshitz, *Quantum Mechanics*, 3rd ed. (Pergamon, Oxford, 1977).

- [13] Here we assume that the electron energy is below the target excitation threshold.
- [14] V. V. Flambaum, A. A. Gribakina, G. F. Gribakin, and M. G. Kozlov, Phys. Rev. A **50**, 267 (1994); V. V. Flambaum, A. A. Gribakina, and G. F. Gribakin, Phys. Rev. A **54**, 2066 (1996); **58**, 230 (1998).
- [15] V. V. Flambaum and O. K. Vorov, Phys. Rev. Lett. **70**, 4051 (1993).
- [16] A. Bohr and B. Mottelson, *Nuclear structure*, Vol. 1 (Benjamin, New York, 1969).
- [17] D. C. Griffin, M. S. Pindzola, and C. Bottcher, Phys. Rev. A **31**, 568 (1985).
- [18] S. Sahoo and G. F. Fribakin, J. Phys.B: At. Mol. Opt. Phys. **36** 3349 (2003).